iomac
International Operational Modal Analysis Conference
11th International Operational Modal Analysis Conference
20 - 23 May 2025 | Rennes, France

Physics-Aware Neural Network Integrated with Stochastic Subspace Identification for Quantification of Physical Changes

Nikhil Mahar [1], *Nikesh Yadav* [1], *Gajendra Yadav* [1], *Subhamoy Sen* [1*], *and Laurent Mevel* [2]

[1] i4S Laboratory, Indian Institute of Technology Mandi, Mandi, HP, India, subhamoy@iitmandi.ac.in

[2] Univ. Gustave Eiffel, Inria, COSYS-SII, I4S Team, France, laurent.Mevel@inria.fr

ABSTRACT

Structural Health Monitoring (SHM) is essential for ensuring the reliability of structural and mechanical components across various engineering domains. Traditional model-based SHM techniques often struggle with complex systems and the limited availability of accurate physical models. On the contrary, data-driven, model-independent approaches, while simple and fast, frequently lack a comprehensive understanding of system physics and suffer from generalization issues. In recent years, Physics-Informed Neural Networks (PINNs) have emerged as a promising alternative that leverages both data and physical models. Despite their success in state estimation for structural systems, limited research has focused on inverse applications. A significant challenge in using PINNs for parameter identification lies in their computational demand. To address this, this study proposes a novel integration of Stochastic System Identification (SSI) and Physics-Informed Neural Networks (PINN) for joint input-state-parameter identification in structural systems (SSI-Pi-LSTM). SSI employs statistical analysis and subspace identification techniques to reliably estimate state-space matrices and dominant modal parameters from structural response data. These parameters can then be incorporated into the PINN framework, reducing estimation time and improving accuracy. This combined approach aims to bridge the gap between efficiency and precision in structural parameter identification.

Keywords: Stochastic System Identification, Finite Element Modeling, Damage Quantification, Eigenstructure, Physics Informed Neural Networks

1. INTRODUCTION

Structural health monitoring (SHM), essential for enhancing infrastructure safety and performance, typically follows two avenues: data-driven and physics-driven approaches. Data-driven strategies generally utilize statistical techniques in either time [1] or frequency domains [2]. Conversely, physics-driven methods use a predefined parameterized model that assimilates knowledge from empirical data

[3]. While data-driven methods rely on statistical distances that often overlook spatial correlations [4], physics-driven strategies, despite integrating physical principles, can encounter computational challenges and stability issues due to model inaccuracies. Nevertheless, progress in machine learning (ML) and artificial intelligence (AI) offers promising solutions to these challenges.

In recent studies, Artificial Neural Networks (ANNs) have been widely utilized to estimate suitably chosen structural parameters that facilitate the evaluation of structural conditions, by interpreting vibrational responses. [5]. A key drawback of these methods is their reliance on extensive data archives to achieve accurate estimations, thereby reducing their practical usage [6]. Alternatively, Physics-Informed Neural Networks (PINNs) [7] offer a robust solution by integrating physical system insights through a supporting model to mitigate sparse measurement challenges.

Research highlighted by [8–10] has proven the effectiveness of PINNs in estimating states and parameters in the context of SHM. Nevertheless, their use in time-domain formulations can be computationally intensive, especially for extensive structures or detailed models. To address this, our study incorporates modal-domain data into the PINN framework, alongside time-domain physics. This approach offers several benefits: (1) lowering computational demands by accommodating modal dynamics in time domain; (2) enhancing noise robustness by utilizing modal parameters in addition to noise-prone time-series responses; and (3) improving the credibility of an otherwise output-only data-driven system identification approach by reinforcing the estimation with system physics. Finally, this study adopts an SSI-based system identification approach that utilizes a data-stacking strategy to reconstruct underlying system dynamics more effectively and has been proven quite effective to estimate modal parameters for civil engineering structures. This paper will recall the fundamentals of the SSI method, then presents the basic foundations of Pi-LSTM to finally propose a fusion of both approaches in a new SSI-Pi-LSTM method that will be validated on a numerical model.

2. STOCHASTIC SUBSPACE IDENTIFICATION (SSI) METHOD

SSI is a well-established method for analyzing and understanding the behavior of dynamic systems. It is a classical system identification technique that constructs a block Hankel matrix from raw measurement data and subsequently applies QR factorization and SVD for dimensionality reduction and system estimation. The dynamics of a vibrating structure can be represented by the following second-order differential equation:

$$\mathbf{M}\ddot{\mathbf{q}}(t) + \mathbf{C}\dot{\mathbf{q}}(t) + \mathbf{K}(\boldsymbol{\lambda})\mathbf{q}(t) = \mathbf{f}(t), \tag{1}$$

where $\mathbf{M}$, $\mathbf{C}$, and $\mathbf{K}$ are the mass, damping, and stiffness matrices, respectively, representing the physical properties of the system. The vectors $\mathbf{q}(t)$, $\dot{\mathbf{q}}(t)$, and $\ddot{\mathbf{q}}(t)$ denote the displacement, velocity, and acceleration responses, while $\mathbf{f}(t)$ represents the external force vector. The equation can be rewritten in a state-space form as

$$\dot{\mathbf{x}}(t) = \mathbf{A}_c\mathbf{x}(t) + \mathbf{B}_c\boldsymbol{u}(t) \tag{2}$$

where

$$\mathbf{x}(t) = \begin{bmatrix}\mathbf{q}(t)^T & \dot{\mathbf{q}}(t)^T\end{bmatrix}^T, \quad \mathbf{A}_c = \begin{bmatrix}\mathbf{0} & \mathbf{I} \\ -\mathbf{M}^{-1}\mathbf{K} & -\mathbf{M}^{-1}\mathbf{C}\end{bmatrix}, \text{ and } \mathbf{B}_c = \begin{bmatrix}\mathbf{0} \\ \mathbf{M}^{-1}\end{bmatrix}.$$

Although Equation (1) accurately describes the behavior of a vibrating structure, it is not directly used in system identification methods due to several practical considerations. First, in real-world applications, it

is often infeasible to measure all degrees of freedom (dofs), and additional noise components beyond $\mathbf{u}(t)$ must be accounted for. Second, the equation is formulated in a continuous domain, whereas experimental measurements are inherently discrete, and sampled at fixed time intervals Δt.

A discrete-time stochastic state-space model effectively addresses these challenges and calculates the modal parameters of a dynamic system. Given an m-dimensional time series as $\{\mathbf{y}_k\}$ wherein $\mathbf{y}_k = \mathbf{y}(t_k)$, where $t_k = k\Delta t$, $k \in \{1, 2, \cdots, S\}$, where S denotes the total sampling points. the structure's dynamic behavior can be modeled using a stochastic state equation under ambient excitations like traffic, waves, and wind:

$$\mathbf{x}_k = \mathbf{A}\mathbf{x}_{k-1} + \mathbf{B}\mathbf{u}_k \tag{3}$$

$$\mathbf{y}_k = \mathbf{H}\mathbf{x}_k + \mathbf{D}\mathbf{u}_k \tag{4}$$

$\mathbf{A} \in \mathbf{R}^{n\times n}$ and $\mathbf{H} \in \mathbf{R}^{m\times n}$ represent the state-space and output matrices, respectively. The state vector $\mathbf{x}_k \in \mathbf{R}^{n\times 1}$ has dimension n, while the output vector $\mathbf{y}_k \in \mathbf{R}^{m\times 1}$. The ambient unmeasured natural force $\mathbf{u}_k$ is assumed to be represented by a centered Gaussian random variable of constant variance. The eigenstructure of the continuous and discrete systems are related by $\exp^{\nu} = \mu$, where μ (resp. ν) is an eigenvalue of $\mathbf{A}$ (resp. $\mathbf{A}_c$).

SSI is particularly suited for output-only identification, where the external excitation is assumed to be stochastic (e.g., white noise) rather than a known deterministic force. The primary step in the SSI approach is projecting a structure's prospective outputs onto the subspace formed by its past outputs to extract only the pertinent historical data necessary for anticipating the structure's future behavior. This selection process decreases the problem's dimensionality and subsequently the algorithm's computational burden. Time-series measurements are arranged in a block Hankel matrix, structuring them such that each block aligns with successive time shifts in the response data. This organization is vital for subspace system identification algorithms, as it encapsulates the fundamental dynamics and interrelationships across various time lags. For a stochastic system, the block Hankel matrix is constructed by scaling the structure's output measurements with a factor $\frac{1}{\sqrt{j}}$, which can be defined as:

$$\mathbf{H}_{0|2i-1} \overset{\text{def}}{=} \frac{1}{\sqrt{j}} \left[\begin{array}{ccccc} \mathbf{y}_0 & \mathbf{y}_1 & \mathbf{y}_2 & \cdots & \mathbf{y}_{j-1} \\ \mathbf{y}_1 & \mathbf{y}_2 & \mathbf{y}_3 & \cdots & \mathbf{y}_j \\ \vdots & \vdots & \vdots & \ddots & \vdots \\ \mathbf{y}_{i-1} & \mathbf{y}_i & \mathbf{y}_{i+1} & \cdots & \mathbf{y}_{i+j-2} \\ \hline \mathbf{y}_i & \mathbf{y}_{i+1} & \mathbf{y}_{i+2} & \cdots & \mathbf{y}_{i+j-1} \\ \mathbf{y}_{i+1} & \mathbf{y}_{i+2} & \mathbf{y}_{i+3} & \cdots & \mathbf{y}_{i+j} \\ \vdots & \vdots & \vdots & \ddots & \vdots \\ \mathbf{y}_{2i-1} & \mathbf{y}_{2i} & \mathbf{y}_{2i+1} & \cdots & \mathbf{y}_{2i+j-2} \end{array}\right] \overset{\text{def}}{=} \begin{bmatrix} \mathbf{Y}_{0|i-1} \\ \mathbf{Y}_{i|2i-1} \end{bmatrix} \overset{\text{def}}{=} \begin{bmatrix} \mathbf{Y}_- \\ \mathbf{Y}_+ \end{bmatrix} \tag{5}$$

The user-defined index i, representing the number of block rows, must be sufficiently larger than the maximum system order. Each block row, consisting of k rows, contributes $2ki$ rows to the matrix $\mathbf{H}_{0|2i-1}$. The number of columns j is typically set to $S - 2i + 1$, ensuring the use of all S samples. It's crucial that j exceeds $2i - 1$. The subscripts $+$ and $-$ signify "past" and "future," respectively. The past and future matrices, $\mathbf{Y}_-$ and $\mathbf{Y}_+$, emerge from separating $\mathbf{H}_{0|2i-1}$ equally into 2 sets of i block rows. The state sequence of a stochastic model is determined by projecting the future output space onto the past, followed by a singular value decomposition. Other SSI approaches can be used, such as the SSI-cov algorithm and its efficient implementation as detailed in [11]. Also, optimal mode selection procedures can be implemented such as those proposed in [12].

To preserve all relevant past information for predicting the future, an orthogonal projection is executed, projecting the row space of "future" outputs into the row space of "past" outputs as expressed below:

$$\mathcal{H} = Proj(\mathbf{Y}_+, \mathbf{Y}_-) = \mathbf{Y}_+\mathbf{Y}_-^T(\mathbf{Y}_-\mathbf{Y}_-^T)^{\oplus}\mathbf{Y}_- \tag{6}$$

where superscript $\oplus$ signifies the moore-penrose pseudo-inverse operation.

The modal properties can then be retrieved as explained in [13], where the observability matrix then the system matrices themselves can be retrieved and estimated thanks to singular value decomposition and least squares.

2.1. SSI integrated with Physics-informed LSTM (SSI-Pi-LSTM)

To assess system health, Equations (3) and (4) are parameterized using location-specific health indicators, $\{\lambda_i\},\ i = 1, \ldots, p$, where p represents the number of monitored locations. Each λ_i quantifies the level of localized stiffness deterioration, with a value of 0 indicating complete structural damage and 1 representing an intact healthy state. System dynamics based on parametrized FEM system matrices $\mathbf{A}(\lambda)$, $\mathbf{B}$, $\mathbf{H}(\lambda)$ and $\mathbf{D}$ can be represented as:

$$\mathbf{x}_k = \mathbf{A}(\lambda)\mathbf{x}_{k-1} + \mathbf{B}\mathbf{u}_k \tag{7}$$

$$\mathbf{y}_k = \mathbf{H}(\lambda)\mathbf{x}_k + \mathbf{D}\mathbf{u}_k \tag{8}$$

To estimate health parameters, modal data from SSI is integrated into an LSTM framework, forming the unified SSI-Pi-LSTM approach. Inspired by Pi-LSTM [14] for structural response estimation, this framework replaces direct differential equation constraints with a physics simulator, ensuring state evolution follows governing physics. This approach, termed Pi-LSTM, is illustrated in Figure 1. In Pi-LSTM, measurement data $\{\mathbf{y}_k\}_{m\times N_h}$ from a time interval N_h ($N_h < S$) is used to predict the unknown forcing function $\tilde{\mathbf{u}}_k$ and estimate parameters $\tilde{\theta}, \tilde{\lambda}$ representing network weights, biases, and health parameters.

In contrast, SSI-Pi-LSTM incorporates two datasets: measurement data $\{\mathbf{y}_k\}_{m\times N_h}$ and the eigenstructure of the SSI-estimated $\mathbf{A}$, denoted as $\widehat{\mathbf{A}}$. As shown in Figure 2, the network consists of an LSTM layer followed by a fully connected neural network (FCNN), which estimates external forces $\tilde{\mathbf{u}}_k$ based on both network parameters $\tilde{\theta}$ and health parameters $\tilde{\lambda}$.

$$\tilde{\mathbf{u}}_k = LSTM(\mathbf{y}_k, \{\tilde{\theta}, \tilde{\lambda}\}) \tag{9}$$

Further predicted $\tilde{u}_k$ is used in physics simulator to predict states thus acting as physics based model inside framework. Assuming the health state can only affect the stiffness parameters, the system dynamics in form of process and measurement equation can be formulated as:

$$\tilde{\mathbf{x}}_k = \mathbf{A}(\tilde{\lambda})\tilde{\mathbf{x}}_{k-1} + \mathbf{B}\tilde{\mathbf{u}}_k \tag{10}$$

$$\tilde{\mathbf{y}}_k = \mathbf{H}(\tilde{\lambda})\tilde{\mathbf{x}}_k + \mathbf{D}\tilde{\mathbf{u}}_k \tag{11}$$

Rewriting measurement equation as:

$$\tilde{\mathbf{y}}_k = \mathbf{H}(\tilde{\lambda})\{\mathbf{A}(\tilde{\lambda})\tilde{\mathbf{x}}_{k-1} + \mathbf{B}\tilde{\mathbf{u}}_k\} + \mathbf{D}\tilde{\mathbf{u}}_k \tag{12}$$

Based on the above equation, the total data loss, which consists of measurement loss and eigenstructure loss, is computed as follows:

$$\mathcal{L}_1(\{\tilde{\theta}, \tilde{\lambda}\}) = \frac{1}{N_h}\sum_{k=1}^{N_h} \|\mathbf{y}_k - \tilde{\mathbf{y}}_k\|_2\ , \tag{13}$$

$$\mathcal{L}_2(\tilde{\lambda}) = \left\|\text{eig}(\widehat{\mathbf{A}}) - \text{eig}(\mathbf{A}(\tilde{\lambda}))\right\|_2 . \tag{14}$$

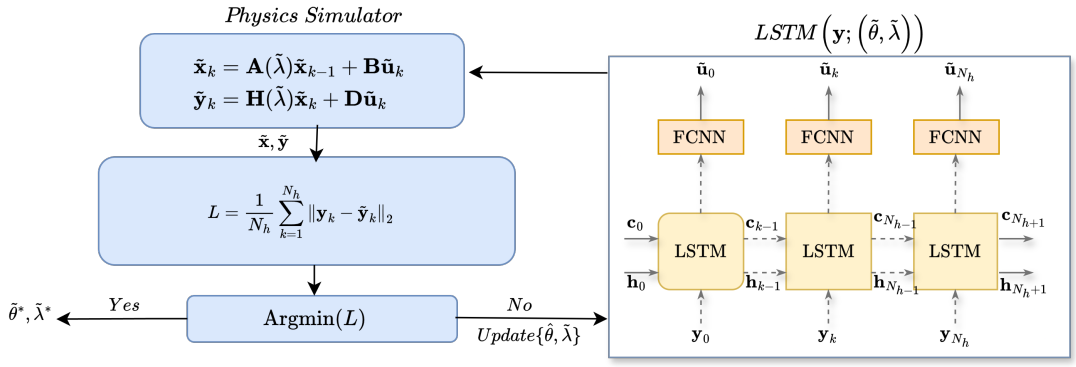

Figure 1: Schematic of Pi-LSTM

The total loss function is thus formulated as:

$$L(\{\tilde{\theta}, \tilde{\lambda}\}) = \alpha \mathcal{L}_1(\{\tilde{\theta}, \tilde{\lambda}\}) + \beta \mathcal{L}_2(\tilde{\lambda}) \tag{15}$$

where α, β are hyperparameters that balance the contributions of different loss terms. While previous studies have investigated optimal selection strategies for these hyperparameters [15], they are set to unity in this study. A self-adaptive weighting approach could be explored in future work to accelerate the training process. The optimization problem for determining the correct neural network and structural parameters $\{\tilde{\theta}, \tilde{\lambda}\}$ is formulated as $\{\hat{\theta}, \hat{\lambda}\} = \arg\min_{\{\tilde{\theta}, \tilde{\lambda}\}} L(\{\tilde{\theta}, \tilde{\lambda}\})$. Notice that the main difference between the new SSI-Pi-LSTM and the classical Pi-LSTM is the inclusion of the norm $\mathcal{L}_2(\tilde{\lambda})$ in the complete loss function, which could be replaced or supplemented by other meaningful information to enhance the convergence efficiency of the algorithm.

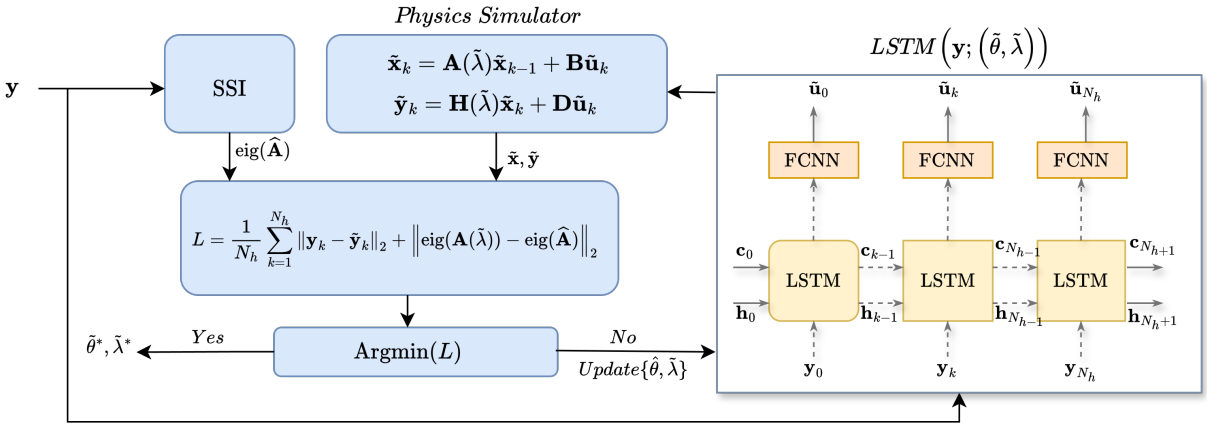

Figure 2: Schematic of SSI-Pi-LSTM

3. NUMERICAL VALIDATION

To validate the proposed framework a a 4-dof spring-mass-dashpot system is adopted. The generalized equation of motion for the dynamics of the system can be perceived from the generalized equation in Equation (1) that imposes the assumed dimension. Accordingly,

$$\mathbf{K} = k_0 \begin{bmatrix} \lambda_1 + \lambda_2 & -\lambda_2 & 0 & 0 \\ -\lambda_2 & \lambda_2 + \lambda_3 & -\lambda_3 & 0 \\ 0 & -\lambda_3 & \lambda_3 + \lambda_4 & -\lambda_4 \\ 0 & 0 & -\lambda_4 & \lambda_4 \end{bmatrix}_{4\times 4}, \quad \mathbf{M} = diag([m_1; m_2; m_3; m_4]),$$

and other system matrices can be defined as follows:

$$\mathbf{A}_c = \begin{bmatrix} \mathbf{0}_{4\times4} & \mathbf{I}_{4\times4} \\ \mathbf{M}^{-1}\mathbf{K} & \mathbf{M}^{-1}\mathbf{C} \end{bmatrix}_{8\times8}, \quad \mathbf{B}_c = \begin{bmatrix} \mathbf{0}_{4\times4} \\ \mathbf{M}^{-1} \end{bmatrix}_{8\times4}$$

In this system, the elements of the diagonal mass matrix are each set to $m_1, m_2, \ldots, m_4 = 126.3$ kg. The initial undamaged stiffness of all springs is assumed to be $k_{0,i} = 84.3$ KN/m for each i. Damping coefficients are determined using Rayleigh damping with a damping ratio of $\zeta = 2\%$. First two natural frequencies along with mass and stiffness of the system, are used to model the damping matrix of the system. The system is considered to have deteriorated in its second, third, and fourth dof. These damages are represented through a set of health indices (HIs), denoted by λ, which quantify the level of deterioration in the spring stiffness on a scale from 0 to 1. Here, $\lambda = 1$ represents a fully healthy spring, while $\lambda = 0$ indicates complete failure. The health indices modify the initial stiffness according to $k_i = \lambda_i k_{0,i}$, where k_i is the effective stiffness of the i-th spring, λ_i is the corresponding health index, and $k_{0,i}$ is the initial undamaged stiffness. With this configuration, the true health indices at each location are represented by the vector $\lambda = \{1, 1, 1, \frac{1}{2}\}$, indicating 50% damage induced at top story. The lumped spring-mass-dashpot model is subsequently simulated under white Gaussian noise $\mathcal{N}(0, 1)$. For parameter identification in these cases, training data consisting of acceleration time histories is generated over a 10-second interval, sampled at a frequency of 50 Hz, with $N_h = 500$. For SSI S=10752 at 200Hz sampling rate.

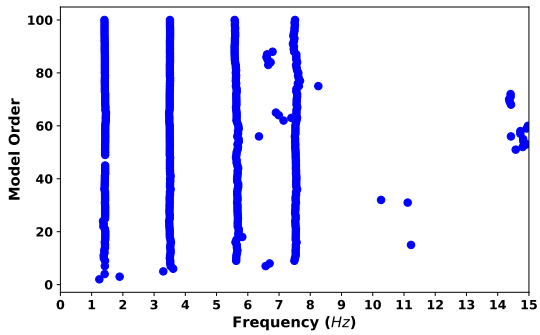

Figure 3: Stabilization Diagram

f_{num} (Hz)	f_{SSI} (Hz)
1.389	1.385
3.472	3.494
5.584	5.661
7.501	7.514

Table 1: Comparison of Numerical and SSI Frequencies

The network architecture for the Pi-LSTM model consists an input layer with 4 neurons, followed by LSTM cell with 128 hidden units. The output of the LSTM cell is passed to a fully connected neural network (FCN) comprising 64 input neurons, 4 hidden layers with 64 neurons each, and a final output layer with 4 neurons. SSI-Pi-LSTM is optimized using the Adam optimizer with a learning rate of 10^{-3}, trained for either 10^5 epochs (i.e. one epoch is a learning iteration in ML terminology) or loss $L(\{\tilde{\theta}, \tilde{\lambda}\})$ becomes less then 10^{-3}. For consistency in comparison, weights and biases (θ) are initialized from a normal distribution, and the structural parameters ($\tilde{\lambda}$) are initialized to 1. Initial hidden ($\mathbf{h}_0$) and cell ($\mathbf{c}_0$) states are set to zero in both models.

A convergence study of Pi-LSTM and SSI-Pi-LSTM was performed with 100% data availability and a 1% signal-to-noise ratio (*snr*). As shown in Figure 4 and Table 2, SSI-Pi-LSTM outperformed Pi-LSTM in accuracy, successfully localizing and quantifying the faulty element. It converged in 37,700 epochs (41 minutes), whereas Pi-LSTM required 86,300 epochs (110 minutes). Additionally, the proposed framework demonstrated reliable state-input-parameter identification.

Numerical modes obtained from both the Pi-LSTM and SSI-PI-LSTM methods are presented in Table 3, alongside a comparison to the reference numerical modes from the model used for data simulation, along with an evaluation of the relative error. Additionally, a noise sensitivity analysis, as shown in Table 4, is conducted to assess the effectiveness of the proposed SSI-Pi-LSTM, with the resulting errors remaining within acceptable limits.

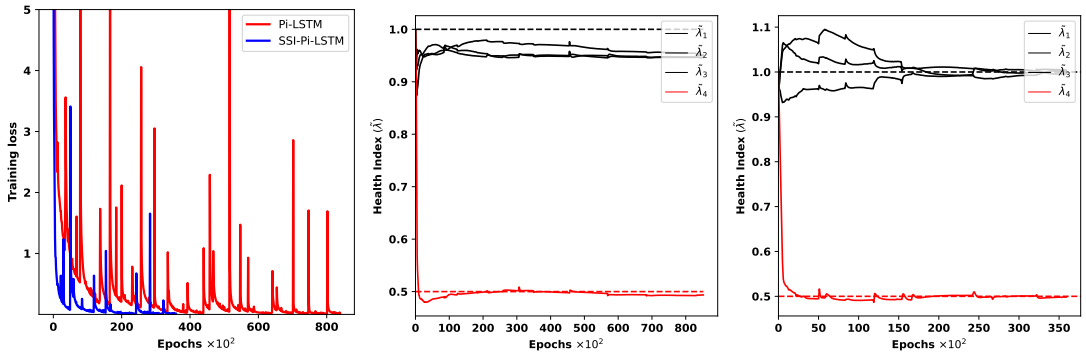

(a) Training loss comparision **(b)** Pi-LSTM **(c)** SSI-Pi-LSTM

Figure 4: Training loss and health indices convergence comparison obtained from Pi-LSTM and SSI-Pi-LSTM

Table 2: Comparison of Pi-LSTM, and SSI-Pi-LSTM for state-input-parameter estimation

DOF	Pi-LSTM					SSI-Pi-LSTM				
	MSE				PE	MSE				PE
	$\mathbf{x}$	$\dot{\mathbf{x}}$	$\ddot{\mathbf{x}}$	$\mathbf{u}$	$\tilde{\lambda}$	$\mathbf{x}$	$\dot{\mathbf{x}}$	$\ddot{\mathbf{x}}$	$\mathbf{u}$	$\tilde{\lambda}$
1	2.5586e-06	1.1033e-06	2.5605e-05	0.1752	4.891	1.0685e-06	9.8434e-07	1.8537e-05	0.0713	0.201
2	6.7453e-06	2.5504e-06	2.6703e-05	0.0690	4.987	3.1517e-06	1.3133e-06	1.1979e-05	0.0896	0.356
3	1.0395e-05	3.7907e-06	2.8530e-05	0.0561	4.122	4.5345e-06	1.8718e-06	1.5569e-05	0.0452	0.412
4	1.5874e-05	5.4091e-06	4.1099e-05	0.0811	1.425	6.1604e-06	3.1587e-06	1.1796e-05	0.0390	0.214

Table 3: Comparison of Numerical, Pi-LSTM, and SSI-Pi-LSTM frequencies with relative Error

f_{num} (Hz)	$f_{Pi-LSTM}$ (Hz)	$f_{SSI-Pi-LSTM}$ (Hz)
1.389	1.355 (**2.45%**)	1.384 (**0.36%**)
3.472	3.401 (**2.04%**)	3.468 (**0.12%**)
5.584	5.467 (**2.10%**)	5.580 (**0.07%**)
7.501	7.301 (**2.67%**)	7.491 (**0.13%**)

Table 4: Noise sensitivity analysis for SSI-Pi-LSTM

DOF	1 % Noise					5% Noise					10% Noise				
	MSE				PE	MSE				PE	MSE				PE
	$\mathbf{x}$	$\dot{\mathbf{x}}$	$\ddot{\mathbf{x}}$	$\mathbf{u}$	λ	$\mathbf{x}$	$\dot{\mathbf{x}}$	$\ddot{\mathbf{x}}$	$\mathbf{u}$	λ	$\mathbf{x}$	$\dot{\mathbf{x}}$	$\ddot{\mathbf{x}}$	$\mathbf{u}$	λ
1	1.0685e-06	9.8434e-07	1.8537e-05	0.0713	0.201	2.2950e-06	5.6255e-06	0.0004	0.4099	1.14	1.5516e-06	1.0171e-05	0.0004	0.5905	0.87
2	3.1517e-06	1.3133e-06	1.1979e-05	0.0896	0.356	7.3034e-06	1.8081e-05	0.0006	0.4561	0.27	4.7119e-06	2.7287e-05	0.0023	0.9425	1.29
3	4.5345e-06	1.8718e-06	1.5569e-05	0.0452	0.412	1.2631e-05	3.3283e-05	0.0007	0.4575	0.11	7.2363e-06	4.6099e-05	0.0015	0.5948	1.76
4	6.1604e-06	3.1587e-06	1.1796e-05	0.0390	0.214	2.1832e-05	7.5131e-05	0.0012	0.8696	0.68	1.0860e-05	1.0592e-04	0.0020	0.4852	0.06

4. CONCLUSION

The numerical study validates the proposed SSI-Pi-LSTM framework for structural health monitoring under unknown excitation and highlights its advantages over the Pi-LSTM algorithm. The convergence history, as shown in Figure 4, demonstrates that the SSI-Pi-LSTM algorithm achieves faster and more reliable physical parameter estimation compared to the Pi-LSTM algorithm, showcasing the benefits of incorporating modal information into the data-based physical learning process. Moreover, the SSI-Pi-LSTM framework accurately identifies input-states-parameters together. Notice finally that any other identification technique could have been used, since this approach is really method agnostic. It has to be noted that the identified parameters provided a good reference to finally obtain a physical estimate close to the desired true value, even for a relatively short time sequence. Further works will include robustness and scale studies for a proper application of this algorithm to real-case studies.

REFERENCES

[1] Michael Döhler, Laurent Mevel, and Falk Hille. Subspace-based damage detection under changes in the ambient excitation statistics. *Mechanical Systems and Signal Processing*, 45(1):207–224, 2014.

[2] Smriti Sharma and Subhamoy Sen. Bridge damage detection in presence of varying temperature using two-step neural network approach. *Journal of Bridge Engineering*, 26(6):04021027, 2021.

[3] Neha Aswal, Subhamoy Sen, and Laurent Mevel. Switching kalman filter for damage estimation in the presence of sensor faults. *Mechanical Systems and Signal Processing*, 175:109116, 2022.

[4] Satish Nagarajaiah and Yongchao Yang. Modeling and harnessing sparse and low-rank data structure: a new paradigm for structural dynamics, identification, damage detection, and health monitoring. *Structural Control and Health Monitoring*, 24(1):e1851, 2017.

[5] Dehao Liu and Yan Wang. Multi-fidelity physics-constrained neural network and its application in materials modeling. *Journal of Mechanical Design*, 141(12), 2019.

[6] YC Liang, DP Feng, and JE Cooper. Identification of restoring forces in non-linear vibration systems using fuzzy adaptive neural networks. *Journal of sound and vibration*, 242(1):47–58, 2001.

[7] Maziar Raissi, Paris Perdikaris, and George E Karniadakis. Physics-informed neural networks: A deep learning framework for solving forward and inverse problems involving nonlinear partial differential equations. *Journal of Computational physics*, 378:686–707, 2019.

[8] Tong Liu and Hadi Meidani. Physics-informed neural networks for system identification of structural systems with a multiphysics damping model. *Journal of Engineering Mechanics*, 149(10): 04023079, 2023.

[9] Marcus Haywood-Alexander, Wei Liu, Kiran Bacsa, Zhilu Lai, and Eleni Chatzi. Discussing the spectrum of physics-enhanced machine learning: a survey on structural mechanics applications. *Data-Centric Engineering*, 5:e30, 2024.

[10] Marcus Haywood-Alexander, Giacomo Arcieri, Antonios Kamariotis, and Eleni Chatzi. Response estimation and system identification of dynamical systems via physics-informed neural networks. *arXiv preprint arXiv:2410.01340*, 2024.

[11] Michael Döhler and Laurent Mevel. Fast Multi-Order Computation of System Matrices in Subspace-Based System Identification. *Control Engineering Practice*, 20(9):882–894, 2012.

[12] Michael Döhler, Palle Andersen, and Laurent Mevel. Variance computation of modal parameter estimates from UPC subspace identification. In *IOMAC - 7th International Operational Modal Analysis Conference*, Ingolstadt, Germany, May 2017.

[13] Peter Van Overschee and Bart De Moor. *Subspace Identification for Linear Systems: Theory, Implementation, Applications*. Springer Science & Business Media, 1996.

[14] Fangyu Liu, Junlin Li, and Linbing Wang. Pi-lstm: Physics-informed long short-term memory network for structural response modeling. *Engineering Structures*, 292:116500, 2023.

[15] Levi D McClenny and Ulisses M Braga-Neto. Self-adaptive physics-informed neural networks. *Journal of Computational Physics*, 474:111722, 2023.